J Polym Res (2015) 22: 175
DOI 10.1007/s10965-015-0823-2

ORIGINAL PAPER

Influence of graphene on thermal degradation and crystallization kinetics behaviour of poly(lactic acid)

Ravibabu Valapa[1] · **Sameer Hussain**[2] · **Parmeswar Krishnan Iyer**[2] · **G. Pugazhenthi**[1] · **Vimal Katiyar**[1]

Received: 2 April 2015 / Accepted: 5 August 2015 / Published online: 13 August 2015

Abstract In present study, the effect of graphene (GR) on crystallization and thermal degradation kinetic behavior of poly(lactic acid) (PLA) was investigated. The non isothermal cold crystallization kinetic study for PLA-GR nanocomposites was carried out using differential scanning calorimetry at different heating rates of 2.5, 5, 7.5 and 10 °C/min. The obtained kinetic data were analyzed using crystallization kinetic models such as Avrami and Tobin methods. The decreasing trend obtained in the Avrami as well as Tobin exponent (n and $n_{T,}$ respectively) with respect to neat PLA revealed the nucleating effect of graphene. Thermal degradation behavior of both PLA and PLA-GR nanocomposites was also analyzed by Kissinger method. The increasing trend in the activation energy with respect to GR loading was observed as compared to neat PLA. This is an indication of improvement in the thermal stability of PLA with an increase in the GR loading. Polarized optical microscopy (POM) was used to observe the growth of spherulites in the PLA and PLA-GR nanocomposites. With respect to addition of GR in the PLA matrix, reduction in the nucleation induction time and an increment in the number of nucleation sites were reflected in the POM analysis.

✉ G. Pugazhenthi
pugal@iitg.ernet.in

✉ Vimal Katiyar
vkatiyar@iitg.ernet.in

[1] Department of Chemical Engineering, Indian Institute of Technology Guwahati, Guwahati, Assam 781039, India

[2] Department of Chemistry, Indian Institute of Technology Guwahati, Guwahati, Assam 781039, India

Keywords Poly(lactic acid) · Graphene · Thermal degradation kinetics · Crystallization kinetics · Kissinger · Avrami · Tobin · Polarized optical microscopy

Introduction

In recent years, bio plastics have been paid significant attention and considered as an effective solution to address the environmental issues spurred by fossil fuel based plastics [1, 2]. At present, poly(lactic acid) (PLA) has become the most commercialized bio-based polyester in the packaging sector owing to its attractive features such as low cost, comparable mechanical and barrier properties with respect to conventional polymers [3]. However, PLA also exhibits low crystallinity and slow crystallization rate, which affects the mechanical strength and barrier effects [3]. In addition to this, PLA displays poor thermal resistance which in turn limits its processing temperature when subjected to practical applications [4–6]. PLA based nanocomposites are aimed at solving the above mentioned limitations.

The current work is focused on understanding the influence of graphene on the crystallization kinetics and thermal degradation behaviour of PLA. Crystallization is considered as one of the prime factors that shows profound impact on the key characteristics such as mechanical and barrier effects of PLA. The effect of graphene on the crystallization behaviour of PLA under isothermal conditions has been documented in the literature [7]. As processing of polymers are carried out under dynamic conditions in practical cases; it becomes essentially worthy understanding the crystallization behaviour of PLA in the presence of graphene under non-isothermal conditions [8, 9]. In view of this, in the current work, non-isothermal cold crystallization behaviour of PLA and PLA-GR nanocomposites is investigated using differential scanning

calorimetry under dynamic heating regime (2.5, 5, 7.5 and 10 °C/min). Further, the experimental crystallization data is analyzed by Avrami model to derive information about the mechanism of nucleation process in PLA and PLA-GR nanocomposites. In addition to this, crystallization rate parameter (CRP) is determined for PLA and PLA-GR nanocomposites using the Avrami parameters (n and K). The influence of GR as nucleating agent and its impact on morphology as well as growth rate of spherulites is performed by polarized optical microscopy (POM) under isothermal crystallization temperature condition (120 °C) at different intervals (5, 10, 15 and 20 min) of cold crystallization process.

Thermal degradation plays a vital role in determining the temperature conditions under which the PLA should be processed [10]. Therefore, it becomes primarily important to investigate the influence of the incorporated graphene on the thermal degradation behaviour of PLA. In the present work, thermo-gravimetric analyzer (TGA) is used as a thermal analysis tool to study the thermal degradation kinetics of PLA and PLA-graphene (PLA-GR) nanocomposites. The PLA and PLA-GR nanocomposites are subjected to thermal analysis under dynamic heating regime (10, 20 and 30 °C) and the effect of GR on the overall kinetics is obtained from the non-isothermal thermal decomposition profile of the composite materials. The solid-state kinetic models proposed for determination of kinetic triplets such as activation energy (E_a), pre-exponential factor (A), and reaction order (n), include both the model-fitting and model-free isoconversional approaches [11]. It has been reported that model-fitting method requires pre-assumption of a kinetic model ($f(\alpha)$) for calculation of kinetic parameters and therefore, produces unreliable Arrhenius parameters [11–14]. Therefore, in the current work, model-free isoconversional Kissinger method is used for determination of kinetic triplets in order to overcome the issues addressed with the model-fitting method.

Experimental

Materials

Expandable graphite (EG, 99.9 %) was donated by Asbury Carbons (USA). Poly(lactic acid) (grade 2003D) obtained from Nature work® was used as the bio-polymer matrix. Chloroform obtained from Merck (India) Ltd., was used as a solvent for synthesizing poly(lactic acid)-graphene (PLA-GR) nanocomposites.

Preparation of PLA-GR nanocomposites

PLA-GR composites were fabricated by solution-casting method as follows: First, PLA (~0.95 g) was dissolved in 30 mL of chloroform with continuous stirring for 2 h in order to completely dissolve the PLA. Graphene exfoliated at 750 °C (0.1, 0.3, 0.5 wt % with respect to PLA) was dispersed in chloroform (20 mL) separately by bath sonication for 30 min. Subsequently, the solution containing dispersed GR was transferred into PLA-chloroform mixture and further subjected to bath sonication for 30 min. Finally, the PLA-GR solution was casted on Teflon petriplates and further, dried under ambient conditions for 24 h. The dried composite films were peeled off carefully from the petriplates. The resulting films were finally oven dried under vacuum for 12 h at 40 °C and stored in airtight bags at room temperature for further characterization. The thickness of the fabricated films was measured using film thickness meter (indi 6156, India). Twenty measurements were taken on each film and the average thickness of the films was found in the range of 60 ± 5 μm. Hereafter, PLA_GR composites prepared with 0, 0.1,0.3 and 0.5(wt%) graphene content were designated as neat PLA, PLA-GR-0.1, PLA-GR-0.3, and PLA-GR-0.5, respectively.

Characterization

Crystallization behavior of PLA and PLA-GR nanocomposites were studied using a differential scanning calorimetry (Mettler Toledo-1 series). Samples (10 ± 0.5 mg) were hermetically sealed in aluminum pans and heated from 25 to 180 °C at various heating rates of 2.5, 5, 7.5 and 10 °C/min in an inert atmosphere (N_2 flow, 50 mL/min). All the samples were first heated from 25 to 180 °C and held at this temperature for 5 min in order to eliminate the effect of thermal and processing history. Glass transition temperature (T_g), cold crystallization temperature (T_{cc}), the enthalpy change at T_{cc} (ΔH_{cc}), melting temperature (T_m) and the enthalpy of fusion at T_m (ΔH_m) for neat PLA and PLA-GR nanocomposite films were determined from the DSC thermograph during the second heating cycle.

Thermogravimetric analysis was performed on a Mettler Toledo thermo gravimetric analyzer (TGA/SDTA 851® model). Samples (10.5 ± 0.3 mg) were placed in 900 μl alumina crucibles and heated from 25 to 700 °C in a 60 ml/min flow of N_2 at heating rates of 10, 20, and 30 °C/min.

The nucleation and spherulite growth in PLA and PLA-GR nanocomposites were observed using Leica DM 2500P polarizing optical microscope fitted with a QICAM FAST1394 camera. The Linkam LTS420 temperature control stage was used to study the morphological changes of the film at isothermal crystallization temperature (120 °C). PLA and PLA-GR nanocomposite films with the thickness of about 60 μm were first melted at 180 °C for 5 min in order to erase thermal histories, and immediately transferred to the temperature of 120 °C for isothermal crystallization. The micrographs of growing spherulites were taken at a specific interval of time before the impingement of spherulites.

Results and discussion

Differential scanning calorimetry analysis

The glass transition, crystallization and melting behaviors of PLA and PLA-GR nanocomposites were investigated from the second heating thermographs obtained using DSC analysis at a heating rate of 5 °C/min (Fig. 1). The T_g value for PLA and PLA-GR nanocomposites does not change significantly. This indicates that the reinforcement of GR in the PLA matrix does not lead to degradation of PLA by stimulating the formation of shorter chain segments [15, 16].

PLA exhibits a unimodal endothermic melting peak at a temperature of ~149 °C suggesting the existence of PLA in α-crystalline arrangement [17–20]. The absence of double melting peak in PLA indicates that only stable crystals of PLA are formed during the cold crystallization process due to the homogeneous nucleation mechanism of PLA. It can be observed that the melting peak of PLA-GR nanocomposites are also characterized by the presence of a unimodal endotherm. This might be probably due to the fact that the addition of GR in the PLA matrix leads to formation of PLA crystals with uniform thickness [21]. In addition to this, shift in the T_m values by ~3–4 °C is noticed for PLA-GR nanocomposites with respect to neat PLA (Table 1). This confirms that GR exhibits nucleation effect, which leads to decrement in the nucleus size as well as growth of thick, stable nucleus in PLA. The shift in the T_m values also indicates that the thermal stability of PLA is enhanced after incorporation of GR. Further, the advancement in the T_m values for PLA-GR nanocomposites reveals that the molecular weight of PLA is not affected by reinforcement of GR and thereby suggesting GR acts as a better nucleating agent. This is also confirmed by the improvement in the crystallinity (%) experienced for PLA-GR nanocomposites with the addition of GR (Table 1).

Non-isothermal cold crystallization kinetics of PLA and PLA-GR nanocomposites

The DSC thermographs of neat PLA and PLA-GR nanocomposites obtained at different heating regime (2.5, 5, 7.5 and 10 °C/min) are analyzed for understanding the non-isothermal crystallization and melting behaviors (Fig. 2). Both PLA and PLA-GR nanocomposites display similar T_g value for a single heating rate. However, the shift in the T_g values is observed for each sample with increasing heating rate, which is attributed to thermal delay [22, 23]. A cold crystallization exotherm is observed in the temperature range of 99–120 °C for neat PLA and 100–126 °C in case of PLA-GR nanocomposites. The steady shift in the T_{cc} to

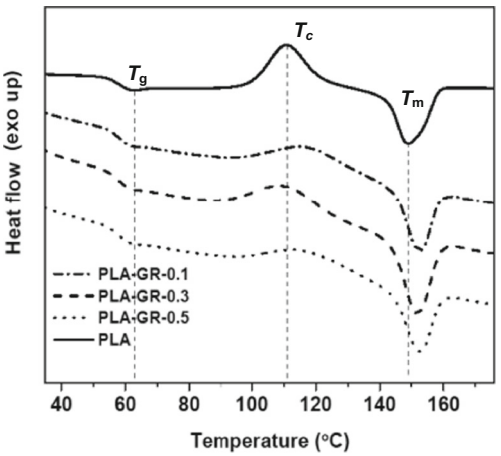

Fig. 1 DSC second heating thermographs for PLA and PLA-GR nanocomposites at a heating rate of 5 °C/min

the greater temperature values with rise in heating rate can be observed for PLA and PLA-GR nanocomposites (Fig. 2). This is ascribed to the lower heat transfer coefficient, which prolongs the time required for cold crystallization process at higher heating rate [24]. A peak corresponding to melting endotherm is noticed for all the samples in the temperature ranging from 150 to 156 °C (Fig. 2). Interestingly, it is observed that all the samples exhibit a double melting endotherm for a heating rate of 2.5 °C/min. The endotherm observed at lower and higher temperature corresponds to the melting phenomenon of imperfect and perfect crystalline structures of PLA developed at the primary and secondary phase of cold crystallization process, respectively [25, 26]. However, the bimodal melting endotherm is not noticed for both PLA and PLA-GR nanocomposites in case of higher heating rates (>2.5 °C/min).

Relative crystallinity

In order to determine the relative degree of crystallinity ($X(t)$), as a function of crystallization time, the exotherms that corresponds to cold crystallization of PLA and PLA-GR

Table 1 DSC results for PLA and PLA-GR nanocomposites

Sample name	T_g (°C)	T_{cc} (°C)	T_m (°C)	T_{mc} (°C)	ΔH_{cc} (J/g)	ΔH_m (J/g)	X_c (%)
PLA	62	110	148	–	16.14	27.2	12
PLA-GR-0.1	63	114	152	100	8.07	25.4	18.5
PLA-GR-0.3	64	113	152.8	101	9.8	27.8	19.2
PLA-GR-0.5	64	110	152.6	101	6.84	23.3	17.5

T_g = Glass transition temperature, T_{cc} = Cold crystallization temperature, T_m = Melting temperature, T_{mc} Melt crystallization temperature, ΔH_{cc} = Enthalpy of cold crystallization, ΔH_m = Enthalpy of melting, X_c = crystallinity (%)

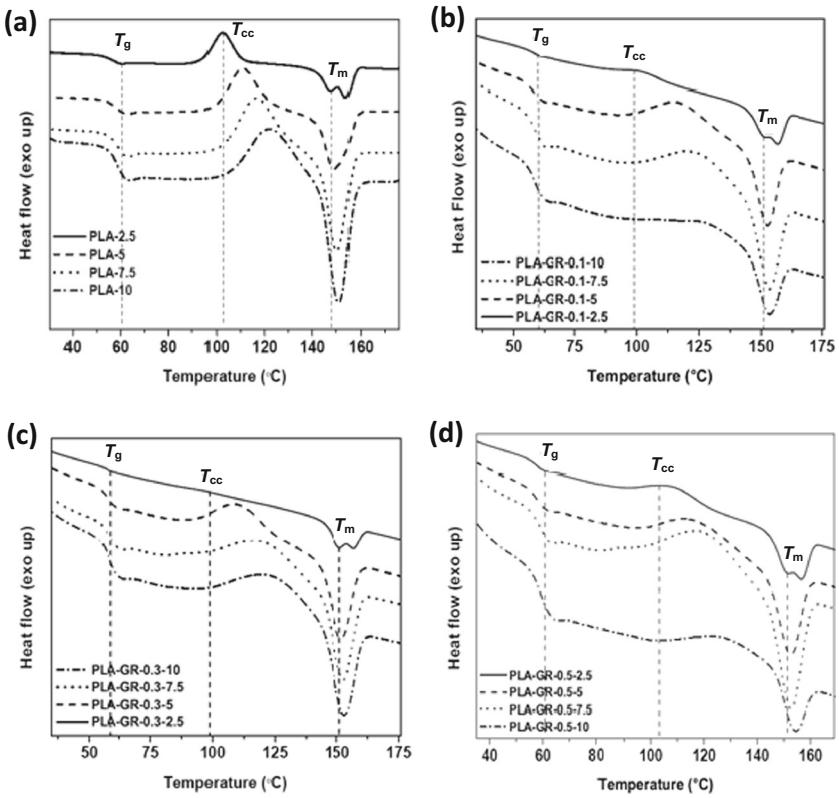

Fig. 2 DSC thermographs at different heating rates of 2.5, 5, 7.5 and 10 °C/min for (**a**) neat PLA, (**b**) PLA-GR-0.1, (**c**) PLA-GR-0.3 and (**d**) PLA-GR-0.5 nanocomposites

nanocomposites are integrated. $X(t)$ as a function of temperature is given by the following equation.

$$X(t) = \frac{\int_{T_0}^{T} \left(\frac{dH_C}{dT}\right) dT}{\int_{T_0}^{T_\infty} \left(\frac{dH_C}{dT}\right) dT} \quad (1)$$

where, T_0 and T_∞ denotes the onset and final cold crystallization temperature respectively [27, 28]. The crystallization time (t) and the respective temperature (T) are related by the following expression

$$t = \frac{T - T_0}{\phi} \quad (2)$$

where, ϕ is the heating rate [27–29]. The values of relative crystallinity are plotted as a function of crystallization time for both neat PLA as well as PLA-GR nanocomposites and the same is portrayed in Fig. 3. The Figure displays a characteristic sigmoidal shaped relative crystallinity curves for all the samples at different heating regime. This discloses the phenomenon of impingement of spherulites that occurred at the advanced phase of cold crystallization process [30]. In addition to this, in case of greater heating rates, the lag effects are not experienced on the crystallization behavior of both PLA and PLA-GR nanocomposites.

Crystallization half-time

The half-time of crystallization ($t_{1/2}$) is defined as the time required to achieve 50 % of crystallization process. Determination of crystallization half-time is of prime importance in understanding the kinetics of crystallization process and is obtained using the following expression [22, 30].

$$t_{1/2} = \left(\frac{\ln 2}{k}\right)^{1/n} \quad (3)$$

The $t_{1/2}$ values obtained for both PLA as well as PLA-GR nanocomposites exhibit downturn with an increase in the heating rates. This is attributed to the faster crystallization completion periods with progress in the heating rate. Also, $t_{1/2}$ values obtained for PLA-GR nanocomposites are noticed to be relatively lower in comparison with neat PLA for all the heating rates. The possible reason for this might be due to the fact that the addition of GR in the PLA matrix accelerates the cold crystallization rate on the whole. The greater $t_{1/2}$ values obtained at the lower heating rate for both PLA and nanocomposite films result from the secondary crystallization phenomenon. In order to study the influence of GR towards the crystallization process, $1/t_{1/2}$ vs ϕ is plotted for PLA and PLA-GR nanocomposites as shown in Fig. 4. One can see that $1/t_{1/2}$ value increases significantly for PLA-GR-0.1 as compared to neat PLA. This increment corresponds to the prominent effect of nucleation ability of GR that stimulates the crystallization

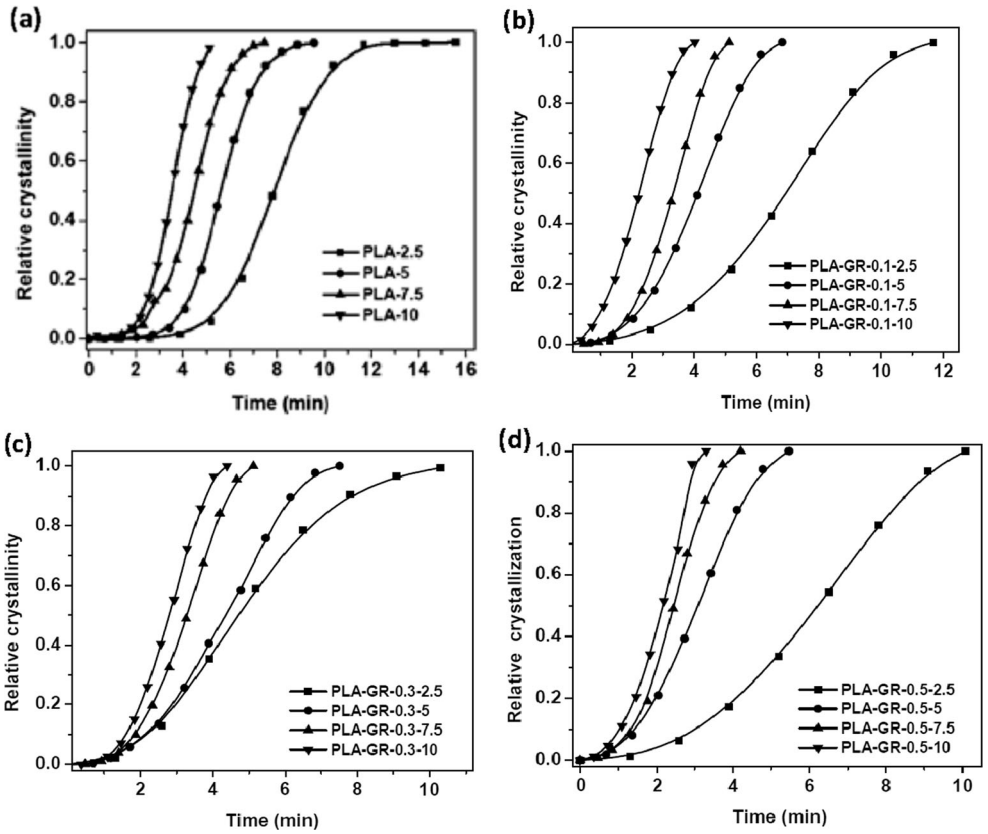

Fig. 3 Relative crystallinity versus crystallization time at different heating rates for (**a**) neat PLA, (**b**) PLA-GR-0.1, (**c**) PLA-GR-0.3 and (**d**) PLA-GR-0.5 nanocomposites

process of PLA. A much profound impact on the $1/t_{1/2}$ values is not evidenced thereafter with further GR loadings in the PLA matrix. However, the increasing trend obtained in the $1/t_{1/2}$ values is ascribed to the nucleation effect of GR resulting in a faster rate of crystallization process in PLA. Further, crystallization rate parameter (CRP) is calculated from the slope of the linear plots shown in Fig. 4, in order to derive quantitative information about the influence of GR on the crystallization rate of PLA. The CRP value for PLA, PLA-GR-0.1, PLA-GR-0.3 and PLA-GR-0.5 is determined to be 0.0272, 0.0372, 0.0404 and 0.0413, respectively. The increasing trend obtained in the CRP values of PLA-GR nanocomposites as compared to neat PLA confirms that reinforcement of GR indeed fastens the cold crystallization process in PLA.

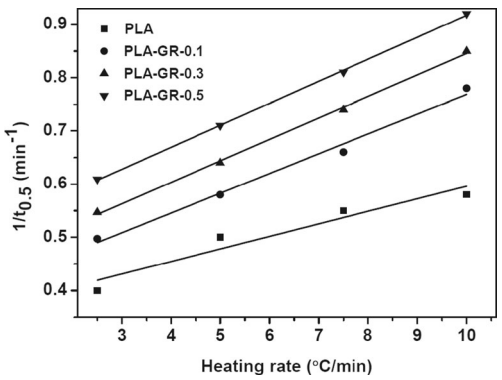

Fig. 4 Effect of GR loading on the crystallization rate parameter (CRP)

Avrami model

The kinetic parameters corresponding to the non-isothermal crystallization process of PLA and PLA-GR nanocomposites are determined using the "Avrami model" and is expressed as follows:

$$X(t) = 1-\exp(-kt^n) \tag{4}$$

The eq. (4) is expressed in the linear form as

$$\log[-\ln(1-X(t))] = \log k + n\log t \tag{5}$$

where, $X(t)$ refers to the relative crystallinity at any time "t", n corresponds to the Avrami exponent, k is the overall kinetic constant [31–33]. The Avrami exponent (n) and the crystallization rate constant (k) are determined using the slope and intercept values obtained from the linear plot of log [− ln (1 - $X(t)$)] vs log t. The relative crystallinity curves corresponding to neat PLA, PLA-GR-0.1, PLA-GR-0.3 and PLA-GR-0.5 are presented in Fig. 3(a-d) and the respective Avrami plots for the same is depicted in Fig. 5(a-d). The linear behaviour exhibited by these plots specifies that the Avrami model adequately elucidates the cold crystallization process of PLA under non-isothermal conditions.

The 'n' values corresponding to Avrami exponent for both PLA and PLA-GR nanocomposites are presented in Table 2. It is apparent that the 'n' values show a decreasing trend with

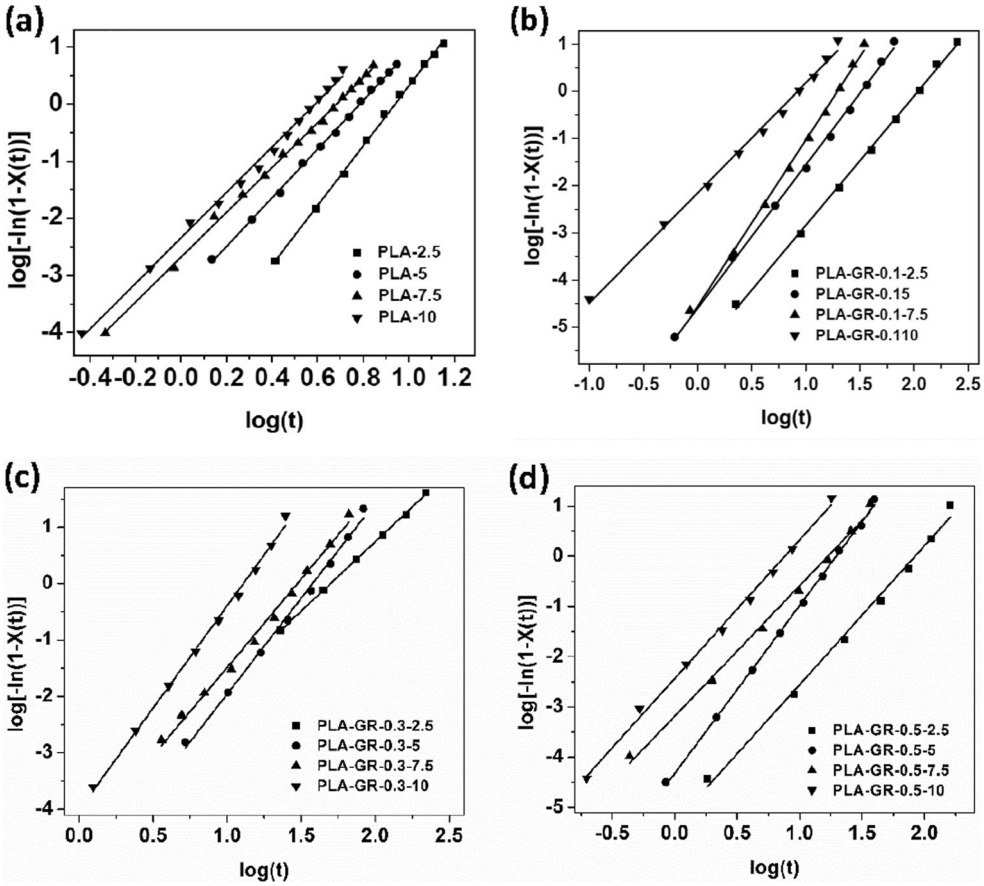

Fig. 5 Avrami plots for non-isothermal cold crystallization of (**a**) PLA, (**b**) PLA-GR-0. 1, (**c**) PLA-GR-0.3 and (**d**) PLA-GR-0.5 nanocomposites

respect to GR loadings in comparison to neat PLA irrespective of the heating rate. The greater 'n' values observed in case of neat PLA is ascribed to the homogeneous nucleation which is responsible for 3-dimensional (3D) growth of PLA crystals [34]. In contrast, the relatively lower 'n' values noticed for PLA-GR nanocomposites suggest that heterogeneous nucleation accelerate the crystallization rate.

Tobin model

The growth site impingement and the secondary crystallization that usually occur during the crystallization process of PLA and PLA-GR nanocomposites cannot be described by Avrami model. This is due to the fact that the Avrami model accounts only for the investigation of initial stage of crystallization progression. Therefore, in order to have an insight into the phase transformation kinetics with growth site impingement, a model proposed by Tobin is utilized for studying the non-isothermal crystallization kinetics of PLA and PLA-GR nanocomposites. The Tobin equation is given by the following expression:

$$X_t = \frac{K_T t^{n_T}}{1 + K_T t^{n_T}} \tag{6}$$

where, X_t refers to the relative crystallinity at time 't', whereas, K_T and n_T are the Tobin parameters related to crystallization rate constant and exponent, respectively [35]. The type of nucleation and growth mechanism associated with the non-isothermal crystallization process of PLA and PLA-GR nanocomposites are derived from the values of Tobin exponent (n_T). The eq. (6) is rearranged as follows:

$$\log\left(\frac{X_t}{1-X_t}\right) = \log K_T + n_T \log t \tag{7}$$

The plot of $\log\left(\frac{X_t}{1-X_t}\right)$ versus log$t$ for PLA and PLA-GR nanocomposites for dynamic heating regime is presented in Fig. 6(a-d). The parameters associated with the crystallization rate (K_T) and Tobin exponent (n_T) are calculated from the slope and intercept values obtained from the linear fit, respectively and is reported in Table 3.

The Tobin exponent (n_T) values for neat PLA are obtained in the range of ~4–6 (Table 3) and the same exhibits a decreasing trend with increasing heating rate. This is in accordance with the values reported in the literature [35]. The crystallization rate parameter 'K_T' values corresponding to the Tobin model demonstrate increasing tendency with respect to heating rate, suggesting the acceleration in the non-isothermal crystallization process of PLA. For PLA-GR

Table 2 Avrami model parameters for PLA and PLA-GR nanocomposites

Sample name	*n*				Log(*k*)			
	2.5 °C/min	5 °C/min	7.5 °C/min	10 °C/min	2.5 °C/min	5 °C/min	7.5 °C/min	10 °C/min
PLA	4.8	4.2	3.9	4.0	−4.9	−3.3	−2.6	−2.3
PLA-GR-0.1	4.2	3.9	3.7	3.6	−3.3	−2.5	−1.9	−1.3
PLA-GR-0.3	4.0	3.4	3.2	3.2	−2.76	−1.85	−1.5	−1.15
PLA-GR-0.5	3.9	3.3	3.2	2.9	−2.3	−1.5	−1.2	−1.01

nanocomposites, the 'n_T'values are found to be in the range of ~3–4 and are comparatively smaller than PLA for all the heating rates studied. The significant variation between the 'n_T'values for PLA and PLA-GR nanocomposites would have been resulted due to the alteration in the crystallization process of PLA. In addition to this, the 'K_T' values obtained in case of PLA-GR nanocomposites show greater deviation from that of the crystallization rate parameter values calculated for PLA, irrespective of the heating rate. This underlines the fact that addition of GR in the PLA matrix leads to noteworthy enhancement in the non-isothermal crystallization progression of PLA. The overall trend noticed in the 'K_T' and 'n_T'values for both the PLA and PLA-GR nanocomposites are in accordance with the trend followed in case of Avrami parameters. This reveals that the physical meaning of Tobin parameters remains the same as the Avrami model.

In crystallization kinetics 'n_T'values shows a significant decrement for PLA-GR nanocomposites compared to neat PLA. In addition to this, 'K_T' values of neat PLA are lesser than the PLA-GR nancomposites, irrespective of the heating time. These two crystallization kinetic parameters indicate that enhancement in the crystallization process of PLA is due to reinforcement of GR. Injection molding is one of the most widely used polymer processing technique. Crystallization kinetics has direct effect on dimensional stability, mechanical and thermal performance of the final product [36]. In this processing technique, polymers should complete the crystallization process before leaving the mould cavity [37]. In such cases, faster crystallization process can have an advantage during fabrication using article throw injection moulding [37].

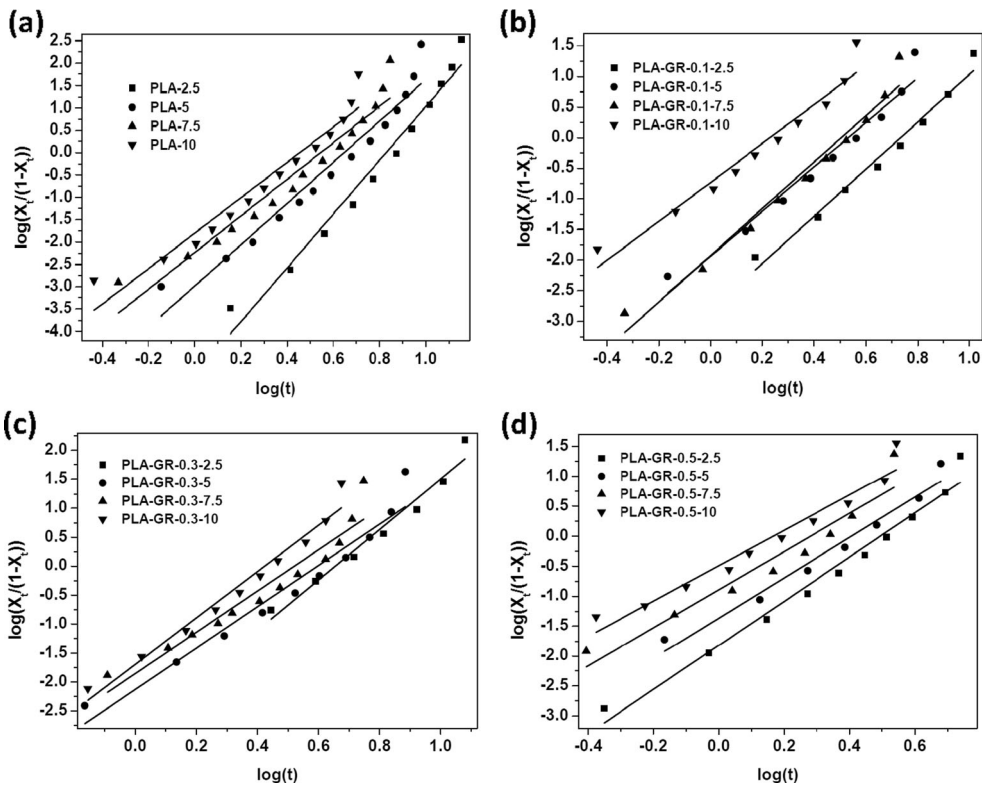

Fig. 6 Tobin plots for non-isothermal cold crystallization of (**a**) PLA, (**b**) PLA-GR-0.1, (**c**) PLA-GR-0.3 and (**d**) PLA-GR-0.5 nanocomposites

Table 3 Tobin model parameters for PLA and PLA-GR nanocomposites

Sample name	n_T				Log(K_T)			
	2.5 °C/min	5 °C/min	7.5 °C/min	10 °C/min	2.5 °C/min	5 °C/min	7.5 °C/min	10 °C/min
PLA	6.0	4.6	4.1	3.9	−5.0	−3.0	−2.3	−1.9
PLA-GR-0.1	3.76	3.65	3.84	2.77	−2.73	−1.99	−1.92	−0.61
PLA-GR-0.3	4.36	3.57	3.56	4.00	−2.85	−2.13	−1.85	−1.69
PLA-GR-0.5	3.67	3.35	3.17	2.94	−1.82	−1.36	−0.89	−0.49

Polarized optical microscopy observations

The influence of GR on the crystallization characteristics of PLA is further explored using polarized optical microscopy (POM) observations under isothermal conditions. Before recording the images, the neat PLA and PLA-GR nanocomposite samples are subjected to heating up to the melting temperature (180 °C) and held under the same environment for a period of 5 min to erase the thermal history. Thereafter, the POM images are taken for PLA and PLA-GR nanocomposites at an isothermal crystallization temperature of 120 °C in various intervals of time (0, 5th, 10th, 15th and 20th min), while cooling from the melt and the respective images are shown in Fig. 7. With addition of GR in the PLA matrix, advancement in the overall crystallization process of PLA is evidenced, which in turn, is confirmed by the reduction in the induction period of nucleation process [38]. Moreover, the dramatic increase in the number of primary nucleation spots with respect to GR loadings is also visualized. Hence, it can be concluded that GR acts as an effective nucleating agent and thereby, fastens the rate of crystallization.

Thermo gravimetric analysis

The temperature-dependent weight loss and derivative of the weight loss profiles for neat PLA and PLA-GR nanocomposites obtained by TGA analysis at a heating rate of 20 °C/min are presented in Fig. 8(a). It can be observed from the Fig. 8(a, b) that both PLA and PLA-GR nanocomposites exhibit two region of weight loss. The initial region of weight loss up to a temperature of around 100 °C is attributed to the pre-adsorbed moisture. The next phase of weight loss that starts above the temperature range of ~300 °C primarily corresponds to intramolecular trans-esterification reaction of PLA [39, 40]. If 10 % weight loss is considered as a reference point for assessment, the corresponding T_{onset} values for neat PLA, PLA-GR-0.1, PLA-GR-0.3 and PLA-GR-0.5 is inferred to be 268, 278, 283 and 299 °C, respectively. The increment in the T_{onset} values of about ~10–31 °C indicates that the thermal stability of PLA is enhanced with respect to GR loadings in the PLA matrix.

Another prime property which should be considered for assessment of thermal stability for a nanocomposite system is the temperature at which maximum rate of weight loss (T_{max}) occurs. The T_{max} value for PLA and PLA-GR nanocomposites is obtained from the first derivative curve of TGA thermograph as shown in Fig. 8(b). In case of both PLA and PLA-GR nanocomposites, a single T_{max} peak is noticed. This reveals that the main degradation of these samples progressed in a single step. Increment in the T_{max} value of ~2 °C is observed for PLA-GR nanocomposites with respect to neat PLA. The GR incorporated in the PLA matrix provides barrier effect for the diffusion of volatile degradation by-products by prolonging the "tortuous pathway" [41, 42]. The advancement in the thermal degradation temperature would also have been resulted from the shielding effect provided by the flake like structure of GR [43].

Thermal degradation kinetics of PLA and PLA-GR nanocomposites

The non-isothermal TGA and DTG curves of PLA and PLA-GR composites at three different heating rates of 10, 20 and 30 °C/min in the nitrogen atmosphere are shown in Figs. 9 and 10, respectively. The TGA curves shown in Fig. 9 reveal that the thermal stability of PLA composites increases with increasing GR content irrespective of the heating rate. The DTG plots reveal the different profiles depending on heating rate and wt% loadings of GR. It can be seen from Fig. 10, that for all the samples, temperatures corresponding to a maximum stage of degradation (T_{max}) increase progressively with increasing the heating rate. The shift of the DTG curves to higher temperatures with an increase in the heating rate could be attributed to the short time provided for a sample to reach a given temperature at a high heating rate [44].

In order to better understand the thermal degradation behaviour of PLA after reinforcement of GR, kinetic studies of degradation process are performed. The thermal degradation kinetics of PLA and PLA-GR nanocomposites can be given by the following expression:

$$\frac{d\alpha}{dt} = kf(\alpha) \tag{8}$$

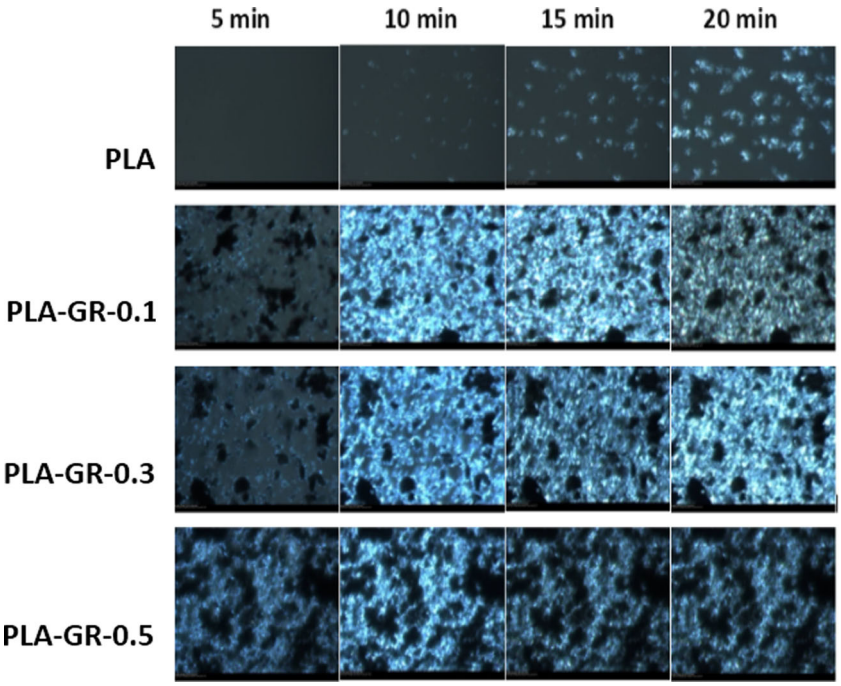

Fig. 7 Optical microscopy images of PLA and PLA-GR nanocomposites with respect to time at 120 °C

where, α corresponds to the degree of conversion or the fraction which is degraded [$\alpha = (w_0\text{-}w_t)/(w_0\text{-}w_f)$, w_0, w_t, and w_f refers to the initial weight, weight remaining at time t, and final weight of the sample, respectively], $d\alpha/dt$ corresponds to the conversion rate, k refers to the temperature-degradation rate constant, and $f(\alpha)$ refers to the kinetic model expressed by differential function, which relies on the specific mechanism for degradation [11, 44].

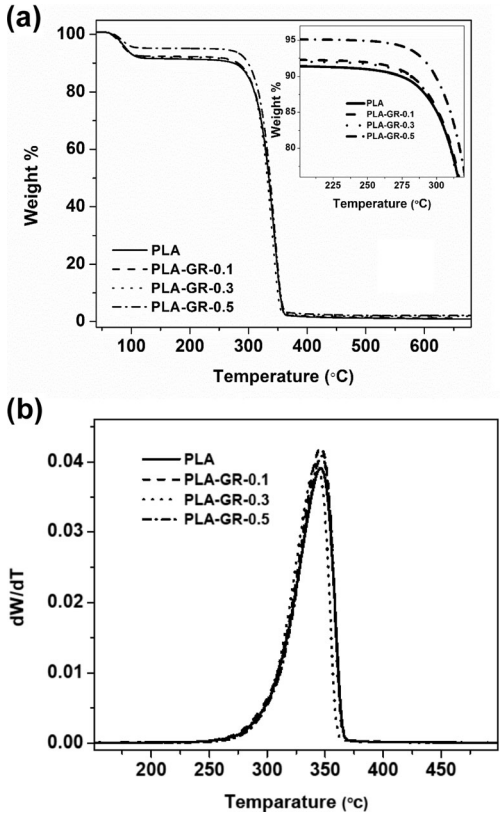

Fig. 8 (**a**) TGA and (**b**) DTG curves of neat PLA and PLA-GR composites

The rate constant (k) that corresponds to temperature dependent degradation can be related to Arrhenius equation by the following expression:

$$k = A\exp\left(\frac{-E_a}{RT}\right) \tag{9}$$

where, A refers to the pre-exponential factor (s^{-1}), E_a corresponds to the activation energy for the degradation process (kJ/mol), R refers to the universal gas constant (8.314 J mol^{-1} K^{-1}), and T corresponds to the absolute temperature (K). In order to derive an expression that helps in understanding the kinetics of degradation process, Eq. (9) is substituted in Eq. (8) and the following expression is obtained.

$$\frac{d\alpha}{dt} = A\exp\left(\frac{-E_a}{RT}\right)f(\alpha) \tag{10}$$

Eq. (10) is useful in predicting the thermal degradation kinetics under isothermal process circumstances, where the samples are subjected to heating at a single heating rate ($\beta = dT/dt$). In the present study, thermal degradation kinetic study of PLA-GR composites is carried out under non-isothermal conditions, where the samples are heated with a constant heating rate (β). Hence, Eq. (10) is altered into an

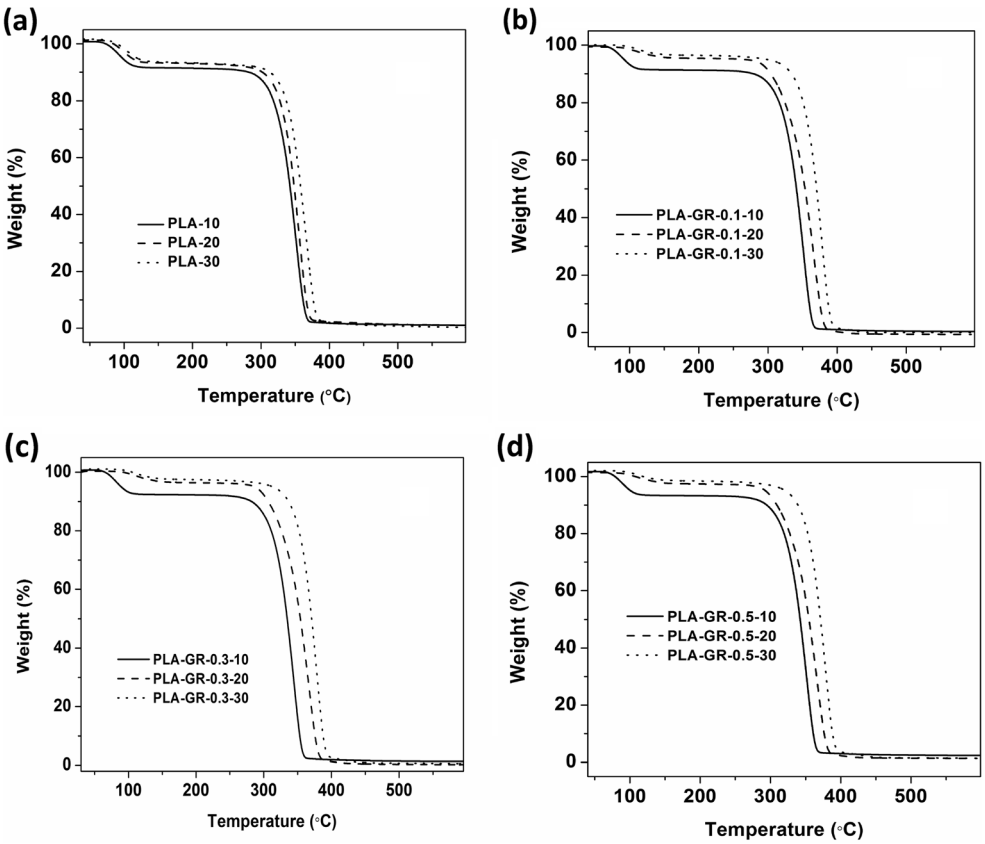

Fig. 9 TGA curves at different heating rates (10, 20, 30 °C) for (**a**) PLA, (**b**) PLA-GR-0. 1, (**c**) PLA-GR-0.3 and (**d**) PLA-GR-0.5 nanocomposites

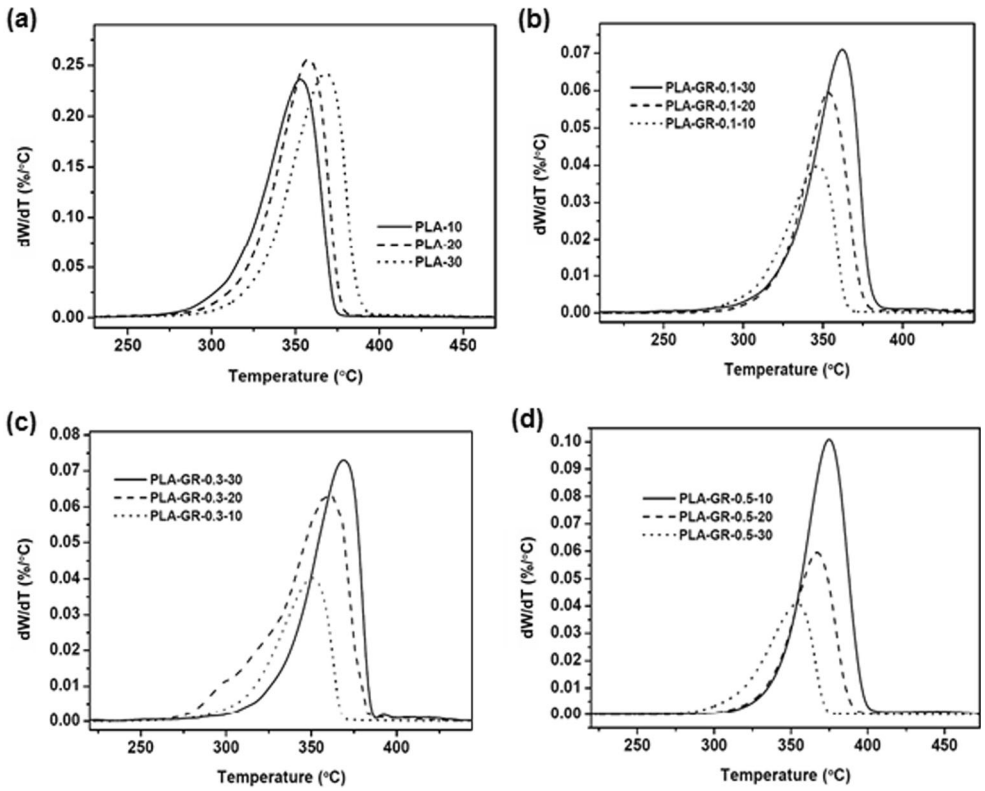

Fig. 10 DTG curves at different heating rates (10, 20, 30 °C) for (**a**) PLA, (**b**) PLA-GR-0. 1, (**c**) PLA-GR-0.3 and (**d**) PLA-GR-0.5 nanocomposites

expression, which defines the rate of degradation with respect to temperature and is given by:

$$\left(\frac{d\alpha}{dT}\right) = \frac{A}{\beta}\exp\left(\frac{-E_a}{RT}\right) f(\alpha) \quad (11)$$

The kinetic triplets for degradation process of polymer nanocomposites based on TGA data can be calculated by using the expressions (Eqs. (10) and (11)) under isothermal and non-isothermal conditions, respectively. For determination of kinetic triplets, the order of reaction for degradation process is assumed to be n^{th} order and $f(\alpha)$, as $(1-\alpha)^n$ [44, 45].

Kissinger method

In the present work, Kissinger method, one of the popular model free approaches is used to acquire knowledge about kinetics of thermal degradation process. The Kissinger method encompasses the advantage of obtaining activation energy at a fixed conversion rate, devoid of any precise awareness regarding the mechanism of thermal degradation reaction from the following expression:

$$\ln\left(\frac{\beta}{T_{\max}^2}\right) = \left\{\ln\frac{AR}{E_a} + \ln\left[n(1-\alpha_{\max})^{n-1}\right]\right\} - \frac{E_a}{RT_{\max}} \quad (12)$$

where, $T_{\max}$, $\alpha_{\max}$, and n refer to the temperature at which maximum weight loss occurs, the degree of conversion corresponding to the inflection point on the TGA thermo graphs and the order of reaction, respectively [46, 47]. The slope that corresponds to the linear plot when $\ln\left(\frac{\beta}{T_{\max}^2}\right)$ is interpreted against $\left(-\frac{1}{T_{\max}}\right)$ is used to calculate the E_a for degradation process.

The apparent activation energy is the primary step to understand the thermal degradation behaviour of PLA-GR nanocomposites. TGA curves obtained at different heating rates of 10, 20, 30 °C/min are used for analyzing the activation energies of the PLA and its nanocomposites. In Kissinger's method, plot of $\ln(\beta/T\ [2]_{\max})$ against $1/T_{\max}$ provides straight lines as shown in Fig. 11. The apparent activation energy is calculated from the slopes corresponding to various straight lines (Fig. 11) and the same is presented in Table 4. As can be seen from Fig. 11, the smooth relativity of the various fitted straight lines shows the feasibility of Kissinger's method. The E_a values obtained from Kissinger method is 177, 179, 181, and 184 for PLA, PLA-GR-0.1, PLA-GR-0.3, and PLA-GR-0.5, respectively. The regression coefficient (R [2]) values obtained in the range of 0.9–0.999 further evidences the applicability of this method for envisaging the thermal degradation behavior of PLA and PLA-GR composites.

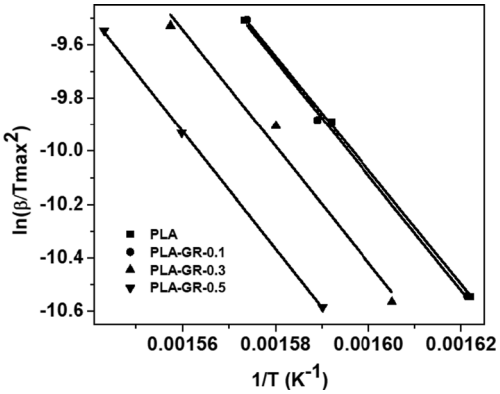

Fig. 11 Kissinger plot for PLA and PLA-GR nanocomposites

Flynn-wall-Ozawa method

The Flynn-Wall-Ozawa method (F-W-O) is one among the integral methods which determine the activation energy for a thermal degradation process without prior knowledge about reaction mechanisms. Activation energy can be obtained directly from weight loss data versus temperature obtained at several heating rates. This method employs Doyle's linear approximation and is denoted by the following expression:

$$\log(\beta) = \left\{\log\frac{AE}{g(\alpha)R} - 2.315\right\} - \frac{0.457E_a}{RT} \quad (13)$$

where β, A, E_a, T, and R are the heating rate, the pre-exponential factor, the apparent activation energy, the absolute temperature, and the gas constant, respectively, and α is the conversion (fractional weight loss). The E_a can be calculated based on the slope of a plot of log (β) versus $-1/T$ for timed value of conversion (α) [48].

Figure 12(a-d) displays the plots of log (β) against $-1/T$ obtained using F-W-O method. The parallel straight lines can be noticed for both PLA and PLA-GR composites at different α values. This indicates the well suitability of F-W-O method for investigating the thermal degradation kinetics at all levels of conversion degree [48, 49]. The plots of activation energy as a function of conversion (α) using the F-W-O method for neat PLA and PLA-GR composites can be seen from Fig. 13.

Table 4 Activation energy and regression co-efficient for PLA and PLA-GR composites obtained by Kissinger method and Flynn-Wall-Ozawa method

S:No	Sample name	Kissinger method		F-W-O method	
		E_a (kJ/mol)	R [2]	E_a (kJ/mol)	R [2]
1	PLA	177	0.999	170	0.995
2	PLA-GR-0.1	179	0.999	178	0.997
3	PLA-GR-0.3	181	0.986	185	0.998
4	PLA-GR-0.5	184	0.997	188	0.996

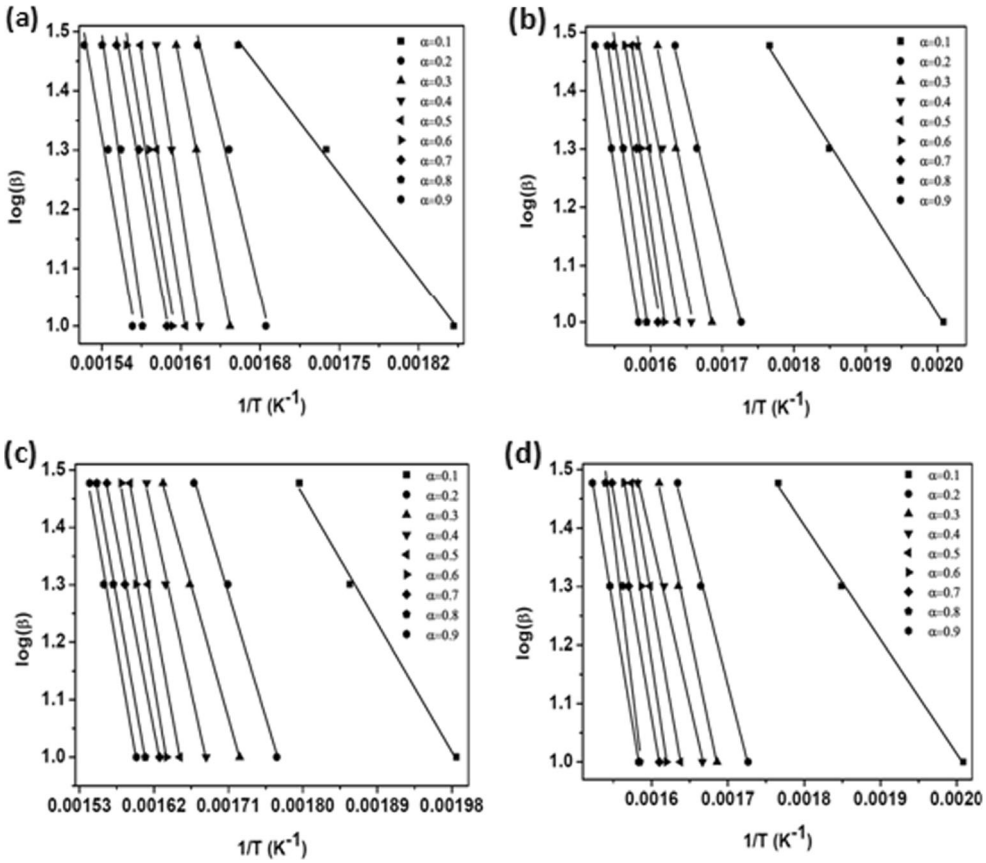

Fig. 12 Flynn-Wall-Ozawa plots for (**a**) PLA, (**b**) PLA-GR-0.1, (**c**) PLA-GR-0.3 and (**d**) PLA-GR-0.5

Variation in the activation energy for both PLA and PLA-GR nanocomposites with respect to conversion can be noticed all through the thermal degradation process. This reveals that the thermal degradation of both PLA and composites does not proceed through the simple process [50, 51]. The activation energy value (177 kJ/mol) obtained for neat PLA is in accordance with the literature data [52]. Increment in the activation energy after the addition of GR in the PLA matrix can be noticed. This indicates that the reinforcement improves the thermal stability of PLA. The E_a values obtained from Kissinger and F-W-O methods are in good agreement with each other. The slight variation arises in the E_a values obtained by both the methods, because, the F-W-O method provides activation energies for various levels of conversion, whereas, the Kissinger method can be applied to only maximum rate of conversion.

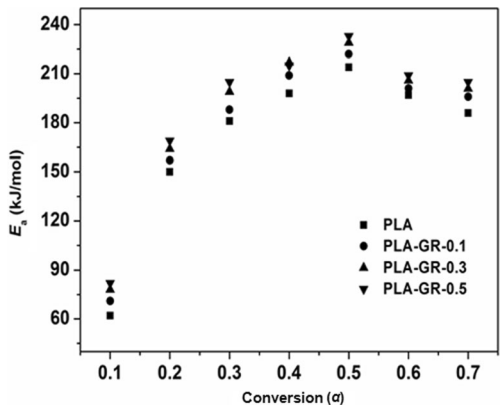

Fig. 13 Conversion versus activation energy for PLA and PLA-GR composites

Conclusions

For both PLA and PLA-GR nanocomposites, the crystallization exotherm shifts to higher temperature side with increasing heating rate, which is indicative of faster rate of the crystallization process. The crystallization rate parameter values of PLA-GR nanocomposites obtained by both Avrami and Tobin models show increasing trend with respect to neat PLA demonstrating the nucleation effect of GR. A similar physical significance provided by both the models suggests the suitability of the same in predicting the crystallization kinetic behavior of PLA and PLA-GR nanocomposites. The nucleating ability of GR in the PLA matrix is revealed by reduction in the nucleation induction period, which is observed by POM studies. After addition of GR in the PLA matrix, thermal stability of PLA is enhanced, which is evidenced by an increment in the activation energy obtained by both the Kissinger and Flynn-Wall-Ozawa methods.

Acknowledgments The authors sincerely thank the Department of Chemicals and Petrochemicals, Ministry of Chemicals and Fertilizers, Government of India funded Center of Excellence for Sustainable Polymers at IIT Guwahati for research facilities to perform this research work.

Ethical agreement

- The manuscript has not been submitted to more than one journal for simultaneous consideration.
- The manuscript has not been published previously.
- A single study is not split up into several parts.
- No data have been fabricated or manipulated.
- No data, text, or theories by others are presented.
- Consent to submit has been received explicitly from all co-authors before the work is submitted.
- Authors whose names appear on the submission have contributed sufficiently to the scientific work and therefore share collective responsibility and accountability for the results.

References

1. Goffin AL, Raquez JM, Duquesne E, Siqueria G, Habibi Y, Dufresne A, Dubois P (2011) From interfacial ring-opening polymerization to melt processing of cellulose nanowhisker-filled polylactide-based nanocomposites. Biomacromolecules 12:2456–2465
2. Ray SS, Bousmina M (2005) Biodegradable polymers and their layered silicate nanocomposites: in greening the 21st century materials world. Prog Mater Sci 50:962–1079
3. Liu H, Song W, Chen F, Guo L, Zhang J (2011) Interaction of microstructure and interfacial adhesion on impact performance of polylactide (PLA) ternary blend. Macromolecules 44:1513–1522
4. Hoglund A, Hakkarainen M, Albertson AC (2010) Migration and hydrolysis of hydrophobic polylactide plasticizer. Biomacromolecules 11:277–283
5. Ljungberg N, Wesslen B, Preparation and properties of plasticized poly(lactic acid) films. Biomacromolecules 6: 1789–1796.
6. Ray SS (2012) Polylactide-based bionanocomposites: a promising class of hybrid materials. Acc Chem Res 45:1710–1720
7. Wu D, Cheng Y, Feng S, Yao Z, Zhang M (2013) Crystallization behavior of polylactide/graphene composites. Ind Eng Chem Res 52:6731–6739
8. Mubarak Y, Harkin-Jones EMA, Martin PJ, Ahmad M (2001) Modeling of non-isothermal crystallization kinetics of isotactic polypropylene. Polymer 42:3171–3182
9. Liu Y, Wang L, He Y, Fan Z, Lia S (2010) Non-isothermal crystallization kinetics of poly(L-lactide). Polym Int 59:1616–1621
10. Tudorachi N, Lipsa R, Mustata FR (2012) Thermal degradation of carboxymethyl starch–g-poly(lactic acid) copolymer by TG–FTIR–MS analysis. Ind Eng Chem Res 51:15537–15545
11. Khawan A, Flanagan DR (2006) Solid-state kinetic models: basics and mathematical fundamentals. J Phys Chem B 110:17315–17328
12. Jankovic B (2008) Solid-state kinetic models: basics and mathematical fundamentals. Chem Eng J 139:128–135
13. Aboyade AO, Carrier M, Meyer EL, Knoetze JH, Gorgens JF (2012) Model fitting kinetic analysis and characterisation of the devolatilization of coal blends with corn and sugarcane residues. Thermochim Acta 530:95–106
14. Jankovic B, Adnadevic B, Jovanovic J (2007) Application of model-fitting and model-free kinetics to the study of non-isothermal dehydration of equilibrium swollen poly (acrylic acid) hydrogel: thermogravimetric analysis. Thermochim Acta 452:106–115
15. Peng F, Shaw MT, Olson JR, Wei M (2011) Hydroxyapatite needle-shaped particles/poly(l-lactic acid) electrospun scaffolds with perfect particle-along-nanofiber orientation and significantly enhanced mechanical properties. J Phys Chem C 115:15743–15751
16. Liu L, Jin TZ, Coffin DR, Hicks KB (2009) Preparation of antimicrobial M membranes: coextrusion of poly(lactic acid) and nisaplin in the presence of plasticizers. J Agric Food Chem 57:8392–8398
17. Katiyar V, Gerds N, Koch CB, Risbo J, Hansen HCB, Plackett D (2010) Poly l-lactide-layered double hydroxide nanocomposites via in situ polymerization of l-lactide. Polym Degrad Stab 95:2563–2573
18. Valapa R, Pugazhenthi G, Katiyar V (2014) Thermal degradation kinetics of sucrose palmitate reinforced poly(lactic acid) biocomposites. Int J Biol Macromol 65:275–283
19. Sawai D, Takahashi K, Sasashige A, Kanamoto T, Hyon SH (2003) Preparation of oriented β-form poly(l-lactic acid) by solid-state coextrusion: effect of extrusion variables. Macromolecules 36: 3601–3605
20. Hoogsteen W, Postema AR, Pennings AJ, Brinke GT (1990) Crystal structure, conformation and morphology of solution-spun poly(L-lactide) fibers. Macromolecules 23:634–642
21. Bharadwaj R, Mohanty AK, Drzal LT, Pourboghrat F, Misra M (2006) Renewable resource-based green composites from recycled cellulose fiber and poly(3-hydroxybutyrate-co-3-hydroxyvalerate) bioplastic. Biomacromolecules 7:2044–2051
22. Ravari F, Mashak A, Nekoomanesh M, Mobedi H (2013) Non-isothermal cold crystallization behavior and kinetics of poly(l-lactide): effect of l-lactide dimer. Polym Bull 70:2569–2586
23. Yasuniwa M, Sakamo K, Ono Y, Kawahara W (2008) Melting behavior of poly(l-lactic acid): X-ray and DSC analyses of the melting process. Polymer 49:1943–1951
24. Nofar M, Zhu W, Park CB, Randall J (2011) Crystallization kinetics of linear and long-chain-branched polylactide. Ind Eng Chem Res 50:13789–13798
25. Fukushima K, Abbate C, Tabuani D, Gennari M, Camino G (2009) Biodegradation of poly(lactic acid) and its nanocomposites. Polym Degrad Stab 94:1646–1655
26. Fortunati E, Armentano I, Zhou Q, Puglia D, Terenzi A, Berglund LA, Kenny JM (2012) Microstructure and nonisothermal cold crystallization of PLA composites based on silver nanoparticles and nanocrystalline cellulose. Polym Degrad Stab 97:2027–2036
27. Pei A, Zhou Q, Berglund LA (2010) Microstructure and nonisothermal cold crystallization of PLA composites based on silver nanoparticles and nanocrystalline cellulose. Compos Sci Technol 70:815–821
28. Vasanthan N, Ly H, Ghosh S (2011) Impact of nanoclay on isothermal cold crystallization kinetics and polymorphism of poly(l-lactic acid) nanocomposites. J Phys Chem B 115:9556–9563
29. Wang L, Jing X, Cheng H, Hu X, Yang L, Huang Y (2012) Blends of linear and long-chain branched poly(l-lactide)s with high melt strength and fast crystallization rate. Ind Eng Chem Res 51:10088–10099
30. Qiu Z, Li Z (2011) Effect of orotic acid on the crystallization kinetics and morphology of biodegradable poly(l-lactide) as an efficient nucleatin. Ind Eng Chem Res 50:12299–12303
31. Bao RY, Yang W, Jiang WR, Liu ZY, Xie BH, Yang MB (2013) Polymorphism of racemic poly(l-lactide)/poly(d-lactide) blend: effect of melt and cold crystallization. J Phys Chem B 117:3667–3674
32. Hemalatha S, Maiti n (2012) Nonisothermal crystallization kinetics of PA6 and PA6/SEBS-g-MA blends. J Polym Res 19:9926–9931
33. Durmus A, Yalcinyuva T (2008) Effect of additives on non-isothermal crystallization kinetics and morphology of isotactic polypropylene. J Polym Res 16:489–498

34. Liao R, Yang B, Yu W, Zhou C (2007) Isothermal cold crystallization kinetics of polylactide/nucleating agents. J Appl Polym Sci 104:310–317
35. Han Q, Wang Y, Shao C, Zheng G, Li Q, Shen C (2013) Nonisothermal crystallization kinetics of biodegradable poly(lactic acid)/zinc phenylphosphonate composites. J Comp Mater 48: 2737–2746
36. Zinet M, Reffa Z, Boutaous M, Xin S, Bourgin P (2013) Thermophysical characterization and crystallization kinetics of semi crystalline polymers. J Mod Phys 4:28–37
37. Andjelic S, Scogna CR (2015) Polymer crystallization rate challenges: the art of chemistry and processing. J Appl Polym Sci 132:42066–42080
38. El-Hadi AM, Mohan SD, Davis FI, Mitchell GR (2014) Enhancing the crystallization and orientation of electrospining poly(lactic caid) (PLLA) by combining with additives. J Polym Res 21:605–612
39. Jayaramudu J, Reddy SMG, Varaprasad K, Saidiku ER, Wang SS, Rajulu AV (2013) Structure and properties of poly (lactic acid)/ sterculia urens uniaxial fabric biocomposite. Carbohydr Polym 94:822–828
40. Wang Y, Steinhoff B, Brinkmann C, Alig I (2008) In-line monitoring of the thermal degradation of poly(l-lactic acid) during melt extrusion by UV–Vis spectroscopy. Polymer 49:1257–1265
41. Cao Y, Feng J, Wu P (2010) Preparation of organically dispersible graphene nanosheet powders through a lyophilization method and their poly(lactic acid) composites. Carbon 48:3834–3839
42. Wang X, Xing W, Zhang P, Song L, Yang H, Hu Y (2012) Covalent functionalization of graphene with organosilane and its use as a reinforcement in epoxy composites. Compo Sci Technol 72:737–743
43. Yu H, Huang N, Wang C, Tang Z (2003) Modeling of poly(L-lactide) thermal degradation: theoretical prediction of molecular weight and polydispersity index. J Appl Polym Sci 88:2557–2562
44. Yuzay IE, Auras R, Valdez H, Selke S (2010) Effects of synthetic and natural zeolites on morphology and thermal degradation of poly(lactic acid) composites. Polym Degrad Stab 95:1769–1777
45. Flynn JH, Wall LA (1966) A quick, direct method for the determination of activation energy from thermogravimetric data. J Polym Sci 4:323–328
46. Chen X, Tu J, Luo Z, Hu S, Zhou Z, Guo S, Lu S (2009) Kinetics of thermo-oxidative degradation of zinc borate/microcapsulated red phosphorous with magnesium hydroxide in flame retarded polypropylene composites. J Polym Res 16:745–753
47. Kissinger HE (1957) Reaction kinetics in differential thermal analysis. Anal Chem 29:1702–1706
48. Chrissafis K (2010) Detail kinetic analysis of the thermal decomposition of PLA with oxidized multi-walled carbon nanotubes. Thermochim Acta 511:163–167
49. Fan Y, Nishida H, Shirai Y, Endo T (2004) Thermal stability of poly (l-lactide): influence of end protection by acetyl group. Polym Degrad Stab 84:143–149
50. Yang TCK, Lin SSY, Chuang TH (2002) Kinetic analysis of the thermal oxidation of metallocene cyclic olefin copolymer (mCOC)/ TiO2 composites by FTIR microscopy and thermogravimetry (TG). Polym Degrad Stab 78:525–532
51. Chen EC, Wu TM (2007) Isothermal crystallization kinetics and thermal behavior of poly(ε-caprolactone)/multi-walled carbon nanotube composites. Polym Degrad Stab 92:1009–1015
52. Li J, Zheng W, Lia L, Zheng Y, Lou X (2009) Thermal degradation kinetics of g-HA/PLA composite. Thermochim Acta 493:90–95